

# Photometric Classification of quasars from RCS-2 using Random Forest

D. Carrasco<sup>1,2</sup>, L. F. Barrientos<sup>1</sup>, K. Pichara<sup>3,4</sup>, T. Anguita<sup>5</sup>, D. N. A. Murphy<sup>1</sup>, D. G. Gilbank<sup>6</sup>, M. D. Gladders<sup>7,8</sup>, H. K. C. Yee<sup>9</sup>, B. C. Hsieh<sup>10</sup>, S. López<sup>11</sup>

1. Instituto de Astrofísica, Pontificia Universidad Católica de Chile, Avenida Vicuña Mackenna 4860, Santiago, Chile
2. School of Physics, University of Melbourne, Parkville, Victoria, Australia
3. Departamento de Ciencia de la Computación, Pontificia Universidad Católica de Chile, Avenida Vicuña Mackenna 4860, Santiago, Chile
4. The Milky Way Millennium Nucleus, Av. Vicuña Mackenna 4860, 782-0436 Macul, Santiago, Chile
5. Departamento de Ciencias Físicas, Universidad Andres Bello, Avenida República 252, Santiago, Chile
6. South African Astronomical Observatory, P.O. Box 9, Observatory 7935, South Africa
7. Kavli Institute for Cosmological Physics, University of Chicago, 5640 South Ellis Avenue, Chicago, IL 60637, USA
8. Department of Astronomy and Astrophysics, University of Chicago, 5640 South Ellis Avenue, Chicago, IL 60637, USA
9. Department of Astronomy and Astrophysics, University of Toronto, 60 St. George Street, Toronto, Ontario M5S 3H8, Canada
10. Institute of Astrophysics & Astronomy, Academia Sinica, Taipei 106, Taiwan, R.O.C.
11. Departamento de Astronomía, Universidad de Chile, Casilla 36-D, Santiago, Chile

## ABSTRACT

We describe the construction of a quasar catalog containing 91,842 candidates derived from analysis of imaging data with a Random Forest algorithm. Using spectroscopically-confirmed stars and quasars from the SDSS as a training set, we blindly search the RCS-2 ( $\sim 750 \text{ deg}^2$ ) imaging survey. From a source catalogue of 1,863,970 RCS-2 point sources, our algorithm identifies putative quasars from broadband magnitudes (g, r, i, and z) and colours. Exploiting NUV *GALEX* measurements available for a subset 16,898 of these objects, we refine the classifier by adding NUV-optical colours to the algorithm's search. An additional subset (comprising 13% of the source catalog) features WISE coverage; we explore the effect of including the W1 and W2 bands on the performance of the algorithm. Upon analysing all RCS-2 point sources, the algorithm identified 85,085 quasar candidates, with a training-set-derived *precision* (the fraction of true positives within the group assigned quasar status) of 90.4% and a *recall* (the fraction of true positives relative to all sources that actually are quasars) of 87.3%. These performance metrics improve for the subset with *GALEX* data; 6,556 quasar candidates are identified with a *precision* and *recall* respectively of 96.9% and 97.3%. Algorithm performance is improved further still with the analysis of WISE data, with *precision* and *recall* further increasing to 99.3% and 99.2% respectively for 21,713 quasar candidates. Upon merging these samples and removing duplicates, we arrive our final catalog of 91,842 quasar candidates. An observational follow up of 17 bright ( $r < 19$ ) potential quasars with long-slit spectroscopy at DuPont telescope (LCO) yields 13 confirmed quasars. Whilst this preliminary sample is small, it signals encouraging progress in the use of Random Forest algorithms to classify point sources for quasar searches within large-area photometric surveys such as the LSST.

*Subject headings:* quasars, surveys, algorithms, photometry

## 1. Introduction

Quasars are important astronomical targets, both individually as cosmic lighthouses and within well-defined quasar catalogues. As such, their classification and identification becomes an important, yet non-trivial task. Their significance in astronomy has led several groups to search and catalogue them. These efforts include: the Large Bright Quasar Survey (LBQS; e.g., Foltz et al. 1989; Hewett et al. 1995), the FIRST Bright Quasar Survey (FBQS; e.g., Gregg et al. 1996; White et al. 2000; Becker et al. 2001), the Palomar-Green Survey of UV-excess Objects (Green et al. 1986), and the FIRST-2MASS Red Quasar Survey (Glikman et al. 2007). Among other applications, quasars can be used to study galaxy evolution (e.g., Hopkins et al. 2006), the intervening intergalactic gas (e.g., Lopez et al. 2008), cosmological evolution (e.g., Oguri et al. 2008), black hole physics (e.g., Portinari et al. 2012) and the analysis of individual galaxies and galaxy clusters due to gravitational lensing (e.g., Faure et al. 2009). The active nuclei of these galaxies produce high luminosities (typically  $\sim 10^{40}$  W) spanning a broad range of frequencies. This spectacular luminosity allows them to be observed at high redshifts, which provides an insight into the distant Universe. Because of their large distances most quasars are observed as point sources in optical surveys, meaning they can easily be misidentified as stellar sources when only photometric information is available. However, by sampling certain rest-frame wavelengths, one may distinguish between local and extragalactic sources through differing spectral characteristics. The lack of a Balmer jump (at 3646 Å rest) in low-redshift ( $z \lesssim 2.2$ ) quasars separates them from the hot star population. The Ly $\alpha$  line emission and absorption characterised by the Ly $\alpha$  forest identified in high-redshift quasar spectra produce broadband colors that progressively redden with redshift (Richards et al. 2002). Most quasar searches are based on only optical colors (e.g., Richards et al. 2001; Bovy et al. 2011); this produces a redshift-dependent bias. This arises from the distinctive strong line emission of quasars. These lines affect quasar colors, distorting the colors expected from the continuum itself. Particularly challenging is the selection of quasar targets at intermediate redshifts ( $2.2 \leq z \leq 3.5$ ), where classification

is typically inefficient. Quasars with magnitudes brighter than  $\sim 21$  are relatively rare, and it can be seen that the quasar and stellar *loci* cross in color space at  $z \sim 2.8$  (e.g., Richards et al. 2002; Bovy et al. 2011).

New methods and approaches in source classification are required to confront the large volume of data, due to be taken over the coming years, from next-generation sky-surveys such as ATLAS (Eales et al. 2010), LSST (LSST Science Collaboration et al. 2009), DES (The Dark Energy Survey Collaboration 2005) and Pan-STARRS (Kaiser et al. 2002). Efficient algorithms are vital in processing these forthcoming data in order to realise the science goals of these surveys; an automated methodology for bulk-classifying the source catalogues will be an essential ingredient to their success.

The main goal of this study is to use a Machine Learning algorithm to construct a catalog of quasars selected from purely photometric information. Machine Learning algorithms have been used to classify objects for many years (e.g., Ball et al. 2006, 2007; Richards et al. 2011). The best known classification models are: decision trees (Quinlan 1993), naive Bayes (Duda and Hart 1973), neural networks (Rumelhart et al. 1986), Support Vector Machines (Cortes and Vapnik 1995), and Random Forest (Breiman 2001). Machine Learning in astronomy, summarized by Ball and Brunner (2010), has found use in star-galaxy separation (e.g., Collister et al. 2007), classification of galaxy morphology (e.g., Huertas-Company et al. 2008), quasar/AGN classification (e.g., Pichara and Protopapas 2013; Pichara et al. 2012), galaxy photometric redshifts (e.g., Gerdes et al. 2010) and photometric redshift estimation of quasars (e.g., Wolf 2009). Our approach for automated quasar identification from only photometric data is based on the Random Forest algorithm (Breiman 2001), which is a Machine Learning algorithm based on multiple decision trees (Quinlan 1993). The application of Random Forests in astronomy is relatively novel, dating back only a few years (e.g.: Dubath et al. 2011; Richards et al. 2011; Pichara et al. 2012). A key strength in the method is an efficient exploration of the spectrum of variable combinations, whilst avoiding arbitrary thresholding to define distinct object classes (such as stars, quasars).

Our search is performed primarily with broadband photometric data from the Red-Sequence

Cluster Survey 2 (RCS-2), in addition to some supplementary data from *GALEX* and WISE surveys. From these data, we construct a catalog of point sources classified as quasars by the Random Forest algorithm. This classification prioritizes the precision over the completeness.

The article is organized as follows: in section §2 we present the data used, including RCS-2, SDSS, WISE, and *GALEX*, in section §3 we describe the Random Forest classifier, along with the training and testing sets used. Section §4 describes the results, and in section §6 we present a discussion and summary of our findings. AB magnitudes are used unless otherwise noted.

## 2. Data

In order to construct a point-source training catalog, we cross-match RCS-2 photometric sources with spectroscopically-confirmed stellar and quasars sources from SDSS. For subsets of this point-source catalog, we merge WISE and *GALEX* photometry. The matching radius depends on the catalogs used. The source catalogs are described below.

### 2.1. RCS-2 dataset

The second Red-Sequence Cluster Survey (RCS-2; Gilbank et al. 2011) is an optical imaging survey that aims to detect galaxy clusters in the  $0.1 \lesssim z \lesssim 1.0$  redshift range. It covers an area of  $\sim 1,000 \text{ deg}^2$ . The data were taken at the CFHT telescope using the MegaCam square-degree imager. The survey was imaged in three filters:  $g'$  (with a  $5\sigma$  point source limiting AB magnitude of 24.4),  $r'$  (limiting magnitude of 24.3), and  $z'$  (limiting magnitude of 22.8). The median seeing in the  $r'$  band is  $0''.71$ . About 75% of the survey area is also observed in the  $i'$  band (limiting magnitude of 23.7) as part of the Canada-France High- $z$  quasar survey (Willott et al. 2005). Our point-source catalog uses all four bands, which means that the area of search is reduced to  $\sim 75\%$  ( $\sim 750 \text{ deg}^2$ ).

Objects are classified according to their light distribution by comparing their curve-of-growth with a weighted average curve derived from a set of four to eight reference PSFs from nearby unsaturated stars. Each source is categorized by object type: 0-artifact/spurious object; 1 or 2-galaxy; 3-

star; 4-saturated (Yee 1991; Yee et al. 1996). All point sources brighter than  $i < 17.5$  are considered as saturated (Gilbank et al. 2011). In this study, we selected type-3 (point-source) objects.

### 2.2. SDSS dataset

The Sloan Digital Sky Survey (SDSS; York et al. 2000) is an optical survey that covers  $\sim 10,000 \text{ deg}^2$  of the sky. The data are obtained at the Apache Point Observatory, with a dedicated 2.5 meter telescope and imaged by a large-format mosaic CCD camera. The optical magnitudes of objects are measured through five optical broad-band filters:  $u'$ ,  $g'$ ,  $r'$ ,  $i'$ , and  $z'$ , designed by Fukugita et al. (1996) with limiting magnitudes of 22.3, 22.6, 22.7, 22.4, and 20.5 respectively in the AB system. The SDSS PSF is typically  $\sim 1''.5$ . We use mainly the data from the Data Release Nine (DR9; Ahn et al. 2012). It is important to clarify that we do not use SDSS magnitudes for the classification.

#### 2.2.1. Quasars

Our source quasar catalogue is derived predominantly from DR9. The DR9 Quasar Catalog contains 228,468 quasar spectra (Ahn et al. 2012). It is this quasar sample we cross-match with RCS-2 point sources to obtain a set of spectroscopically confirmed quasars with RCS-2 photometry.

#### 2.2.2. Stars

Our catalog of stars originates mainly from spectroscopic confirmations of sources in SDSS Data Release 9. The catalog contains 668,054 confirmed stellar spectra (Ahn et al. 2012). We cross-match this combined sample of stars to RCS-2 point source photometry in order to create a catalog of spectroscopically-confirmed RCS-2 stars.

### 2.3. WISE dataset

The Wide-Field Infrared Survey Explorer (WISE; Wright et al. 2010) is an infrared all sky survey. It has four mid-IR bands: W1 at  $3.4 \mu m$ , W2 at  $4.6 \mu m$ , W3 at  $12 \mu m$ , and W4 at  $22 \mu m$  with angular resolutions of  $6''.1$ ,  $6''.4$ ,  $6''.5$ , and  $10''.1$  respectively. Limiting magnitudes (in Vega) are 16.5 for W1, 15.5 for W2, 11.2 for W3, and 7.9 for W4; in our study we will use the W1 and W2 bands, following the approach by Stern et al.

(2012), as mentioned in §3.1.3. For consistency, we convert these magnitudes to the AB system following Tokunaga and Vacca (2005) and Jarrett et al. (2011).

#### 2.4. GALEX dataset

The *Galaxy Evolution Explorer* (GALEX; Martin et al. 2005) is an orbital space telescope with a mission to compile an all-sky photometric map in the UV. The telescope images simultaneously with two bands: the far ultraviolet (FUV; effective wavelength 1528 Å with angular resolution 4".0) and the near ultraviolet (NUV; effective wavelength 2271 Å with angular resolution 5".6). For the 26,000 deg<sup>2</sup> All Sky-Imaging (AIS) catalog, 100-second exposures result in limiting (AB) magnitudes of 19.9 and 20.8 for the FUV and NUV respectively. Whilst there are other deeper GALEX catalogs targeting specific regions, we omit them in preference for a catalog of uniform depth. In this study, we use the data from GR4/5. Because reddening due to galactic dust becomes significant in the UV, we correct each GALEX magnitude with the Schlegel et al. (1998) dust maps based on the extinction law from Cardelli et al. (1989).

### 3. Random Forest

The Random Forest algorithm (Breiman 2001) is a tree-based classification method that learns how to classify objects into different classes using a training set. In this context, training sets are groups of objects with a known classification; each object is characterised by a vector whose components are attribute values. The training set is used to build a model describing how the classes depend on the values of the vector components.

This model is subsequently applied to a database containing objects (with the same attributes) of unknown type in order to make a prediction of the class they belong to. For a training set of  $N$  objects with  $F$  attributes describing the objects, we define  $T$  as the number of trees in the Random Forest and  $M \ll F$  as the number of random features used in the classification process ( $T$  and  $M$  are model parameters). The training procedure is as follows:

- Generate  $T$  data sets with  $N$  objects. Each

dataset is created by randomly sampling objects from the original training set, but with replacement.

- From each of the  $T$  data sets, grow a full<sup>1</sup> decision tree, but on each node select the best split from a set of  $M$  features selected randomly from the  $F$  initial features.

Every tree from the forest can assign a class to an object, based on the attribute values it has. The algorithm's final predicted classification for a given object is that selected by the majority of the  $T$  trees. Operating in this manner, the Random Forest algorithm runs efficiently on large databases and can handle  $F \sim 10^3$  attributes.

To test the classifier we use a 10-fold cross-validation across the training set. This involves partitioning the training set into 10 equal subsets. For a selected subset, we train the model with the other 9 subsets and test the performance of the resultant classifications when applied to this selected subset. This procedure is carried out for each of the 10 subsets. Results from each of these cross-validated runs are analysed with performance metrics. To quantify the performance of the algorithm, for each class of object (**ie. stellar and QSO in this case**) we use *recall* ( $r$ ), *precision* ( $p$ ), and *F-Score* ( $F_s$ ), defined as:

$$F_s = 2 \times \frac{p \times r}{p + r}$$

where:

$$p = \frac{t_p}{t_p + f_p} \quad r = \frac{t_p}{t_p + f_n}$$

$t_p$ ,  $f_p$  and  $f_n$  are the number of true positives, false positives and false negatives respectively.

*Recall* therefore corresponds to the fraction of correctly classified objects of each class with respect to all objects genuinely belonging to that class. *Precision* is the fraction of correctly classified objects within each class compared to with respect to all objects classified by the algorithm as members of that class. *F-score* is the harmonic mean of *precision* and *recall*.

<sup>1</sup>A full decision tree means that there is no pruning of the tree during the construction.

### 3.1. Training Sets

Training sets are samples of objects for which the target class is known. In this study, the classes (stellar and QSO sources) are obtained by cross-identification of SDSS spectroscopically-confirmed targets to RCS-2 point sources, as discussed above in §2.2.1 and §2.2.2. A match between the two catalogs is obtained when their angular positions are separated by less than  $0''.5$ . The cross-matching is performed for both stellar and QSO sources, with respectively 20,659 and 8,762 matches made. From this preliminary matched catalogue we require RCS-2 targets to have measured flux in all four filters, and photometric errors of less than 0.1 in each. Our catalogs consequently reduce in size to 4,916 quasars and 10,595 stars. From these data, we create three different training sets. Each object within the training set is described by attributes of magnitude and colour. We include all possible attributes to open the parameter space available for the algorithm to ensure an optimal classification.

To create the cleanest possible QSO catalog from the Random Forest algorithm, we select the run with the highest *precision* that also has  $F_s \geq 86.0\%$ . This ensures a *recall* above 75%, below which we consider the catalog unacceptably incomplete.

#### 3.1.1. Training Set 1 (TrS1)

As discussed above, we create three training sets from the cross-matched catalog. The first training set features the four bands from RCS-2:  $g'$ ,  $r'$ ,  $i'$ , and  $z'$ ; and the colors  $g-r$ ,  $g-i$ ,  $g-z$ ,  $r-i$ ,  $r-z$ , and  $i-z$ . The most relevant colors are  $g-r$ ,  $r-i$ ,  $i-z$ . Following Richards et al. (2002), it is possible to separate quasars and stars without spectroscopic information by constructing color-color diagrams. In Figure 1 we clearly see the characteristic stellar *locus* and a *clump* of quasars. Despite these attributes being sufficient to split the two classes, as discussed above we nevertheless add all color and magnitude data.

Figure 2 shows the large redshift range of QSOs from this sample: from 0 to 6 and peaking at  $z \sim 2.5$ . In color-color plots, the quasar population lying near this redshift peak can be contaminated with stars, making separation of the two populations more difficult (e.g.: Fan 1999; Richards et al.

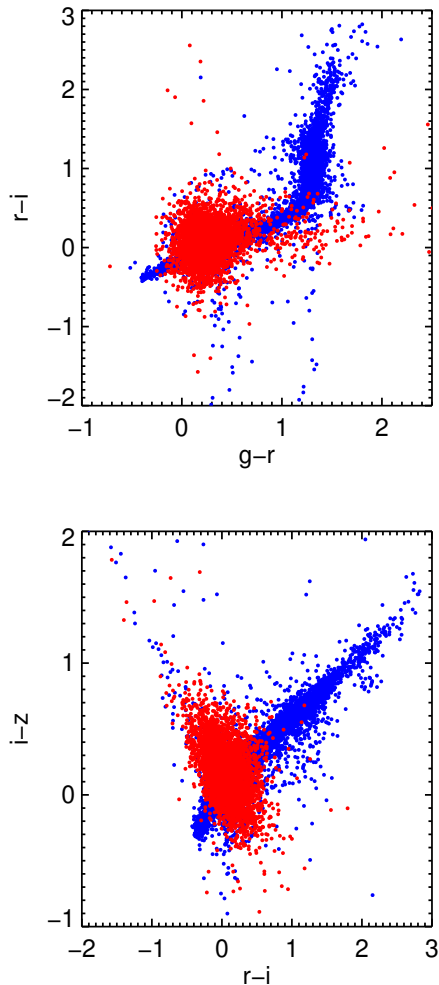


Fig. 1.— Color-color diagrams of spectroscopically confirmed quasars (red) and stars (blue) in RCS-2. The upper diagram shows the colors  $g-r$  vs  $r-i$ , and the bottom diagram shows the colors  $r-i$  vs  $i-z$ . It is possible to see a quasar *clump* and a stellar *locus*, but there is not a clear separation between them.

2002; Bovy et al. 2011). It is important to analyze magnitude distributions, as fluxes might be important attributes in distinguishing stars from quasars. Figure 3 therefore shows the magnitude distribution of stars (blue) and quasars (red), with the former peaking brighter than the latter. This means the training set is biased against faint objects.

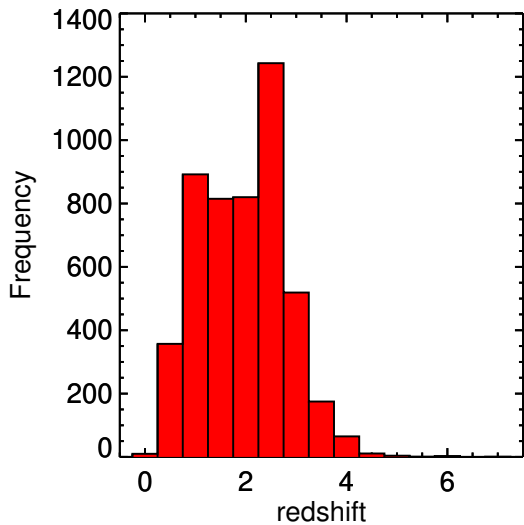


Fig. 2.— Histogram of the redshift distribution of the quasars in TrS1.

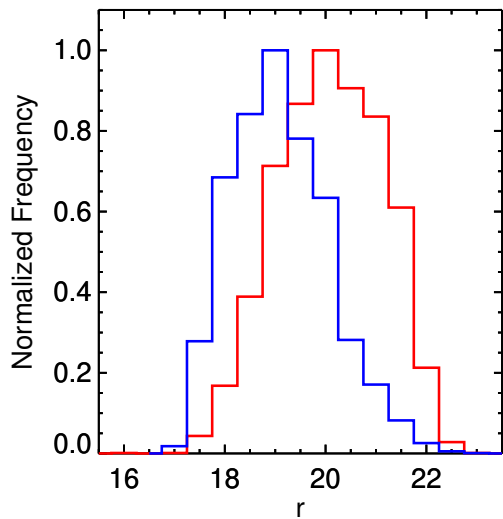


Fig. 3.— Histogram of the normalized magnitude distribution in the  $r$  band from RCS-2 of quasars and stars from TrS1. Quasars are in red and stars are in blue. The peak is 1 magnitude brighter in the case of stars.

We run the model built by the algorithm on the dataset of objects to be classified in order to determine how much this bias influences the result,

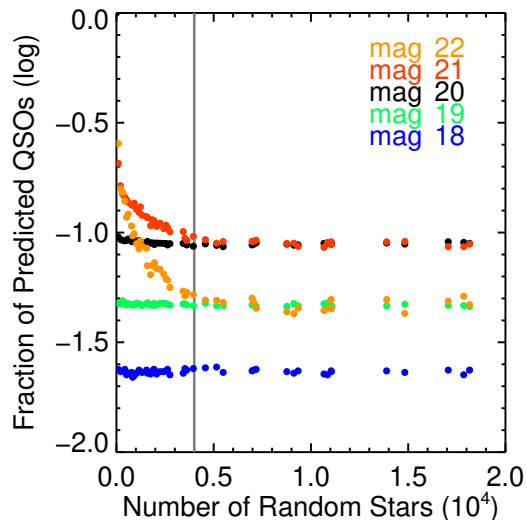


Fig. 4.— Relation between the fraction of predicted quasars from the test set corresponding to TrS1 as function of the point sources added as artificial stars to TrS1.

and then we compare the results to the predictions of LSST (LSST Science Collaboration et al. 2009). It is important to take into account that this prediction is just an upper limit for the number of quasars we expect to find, since our sample is not complete (for example, the training set is biased because it comes from SDSS), and also because we are prioritizing the *precision*, so it is normal to miss some quasars. For magnitudes  $r \gtrsim 20.5$ , we find the number of quasars is overestimated relative to that predicted for the LSST up to the magnitude limit for our data set ( $r \sim 23$ ). We find a similar trend in the training set of classified sources; this arises because the fraction of stellar sources drops off faster than the fraction of QSOs towards fainter magnitudes. Moreover, the predominance of bright ( $r \leq 22$ ) objects within the training set introduces an observational bias that hinders accurate classification of faint objects (up to the catalog magnitude limit of  $r \sim 23$ ). To address this excess of quasar classifications, leading to possible misidentifications at faint magnitudes, we add random  $r \geq 20.5$  point sources from the RCS-2 catalog to the training set and we label them as stars (hereafter, *artificial stars*). Whilst it is inevitable that some artificial stars could in

fact be quasars, we reiterate that our primary aim is of maximising the *precision* rather than *recall*; missing genuine quasars is not as important as reducing the level of stellar contamination in our quasar catalog, particularly at faint magnitudes. To choose an appropriate number of artificial stars ( $N_{\text{ar}}$ ) to add to the training set, we run the algorithm, apply it to the dataset of unclassified objects, and then calculate the fraction of predicted quasars between  $r = 18$  and  $r = 23$  in bins of 1 magnitude.

We repeat this process, gradually adding artificial stars up to  $N_{\text{ar}} \sim 18,000$ . In this manner, we may determine the aforementioned quasar detection fraction as a function of the number of artificial stars added to the training set, as seen in Figure 4. We seek  $N_{\text{ar}}$  such that the predicted quasar fraction is flat across all magnitudes up to the flux limit. As anticipated, Figure 4 shows an always-constant fraction for magnitudes  $r \leq 20$  because the sample is complete in this bright regime. For fainter ( $r \gtrsim 20.5$ ) magnitudes however, we see a decay in the fraction of quasar candidates when adding artificial stars; we are diminishing the number of misclassified stars. We therefore adopt a number of artificial stars to stabilize the quasar candidate fraction. We achieve this by iterating until the standard deviation is smaller than the standard deviation for bright objects ( $r \leq 20.5$ ). From this approach, we determine that 4,000 artificial stars are optimal for our purposes here, corresponding to the black vertical line in Figure 4. Our TrS1 Training Set therefore comprises 4,916 quasars and 14,595 stars, 4,000 of which are artificial stars.

### 3.1.2. Training Set 2 (TrS2)

TrS2 is a subset of TrS1. We cross-identify all quasars and stars from TrS1 with *GALEX* objects detected in the NUV band and with a photometric error of  $\leq 0.25$  (consistent with magnitudes of  $\sim 22.5$ , around the limit magnitude in this band). The search radius used to match sources was  $2''.0$ , based on the angular resolution of both surveys. This cross-matching yields a sample of 1,228 quasars and 815 stars; we note a significant decrease in the number of objects in the catalog, especially stars. We attribute this to both the lower angular resolution of *GALEX* with respect to SDSS/RCS-2, and to the redshift dependence

of the UV emission from quasars: only QSOs with redshifts up to  $z \sim 2.0$  should be detectable via observed-frame spectral features lying within the filter passband. Because stellar emission in the UV is typically low, there are considerably fewer stellar sources in this catalog.

Inclusion of the *GALEX* NUV band is relevant, because optical observations alone do not allow a clean separation between quasars and stars (See Figure 1), especially at intermediate redshifts ( $2.2 \lesssim z \lesssim 3.5$ ). UV flux data are very useful in quasar classification because stellar-QSO populations are well separated in UV-optical color-color space (Trammell et al. 2007). In Figure 5 we can see the color-color diagrams of the quasars and stars with detections in the NUV band. Comparing the NUV-g vs. g-r plot to optical equivalents, we note the overlap between quasars and stars has almost disappeared.

There is a relation between NUV detection of quasars and redshift. An important contribution to the bolometric flux is an intense, broad emission feature dominating the spectral energy distribution (SED) at bluer wavelengths: the so-called big blue bump (Sanders et al. 1989). According to Trammell et al. (2007), NUV-band detections of quasars are almost complete up to  $z \sim 1.4$ , and are still well recovered at  $z \sim 1.7$ . However, by  $z \sim 2.0$  the detection completeness declines to 50%. While it is not clear whether the FUV band or NUV band is best suited for quasar detection, we use just NUV due to the small number ( $\sim 10\%$ ) of NUV-detected sources having FUV fluxes as well. Moreover, the redshift range sampled by FUV sources appears smaller. Figure 6 shows TrS2 redshift coverage is complete only out to low redshifts compared to TrS1 (as seen in Figure 2). Moreover, the limit of r-band magnitudes (Figure 7) is much brighter than TrS1, suggesting the lack of faint-magnitude stars is not a main problem in this training set.

For training set TrS2, the features used for Random Forest classification are the four magnitudes from RCS-2 bands: g, r, i, and z; the NUV band; and the colors: NUV-g, NUV-r, NUV-i, NUV-z, g-r, g-i, g-z, r-i, r-z, and i-z. As discussed in §3.1, all color combinations are added for analysis by the algorithm.

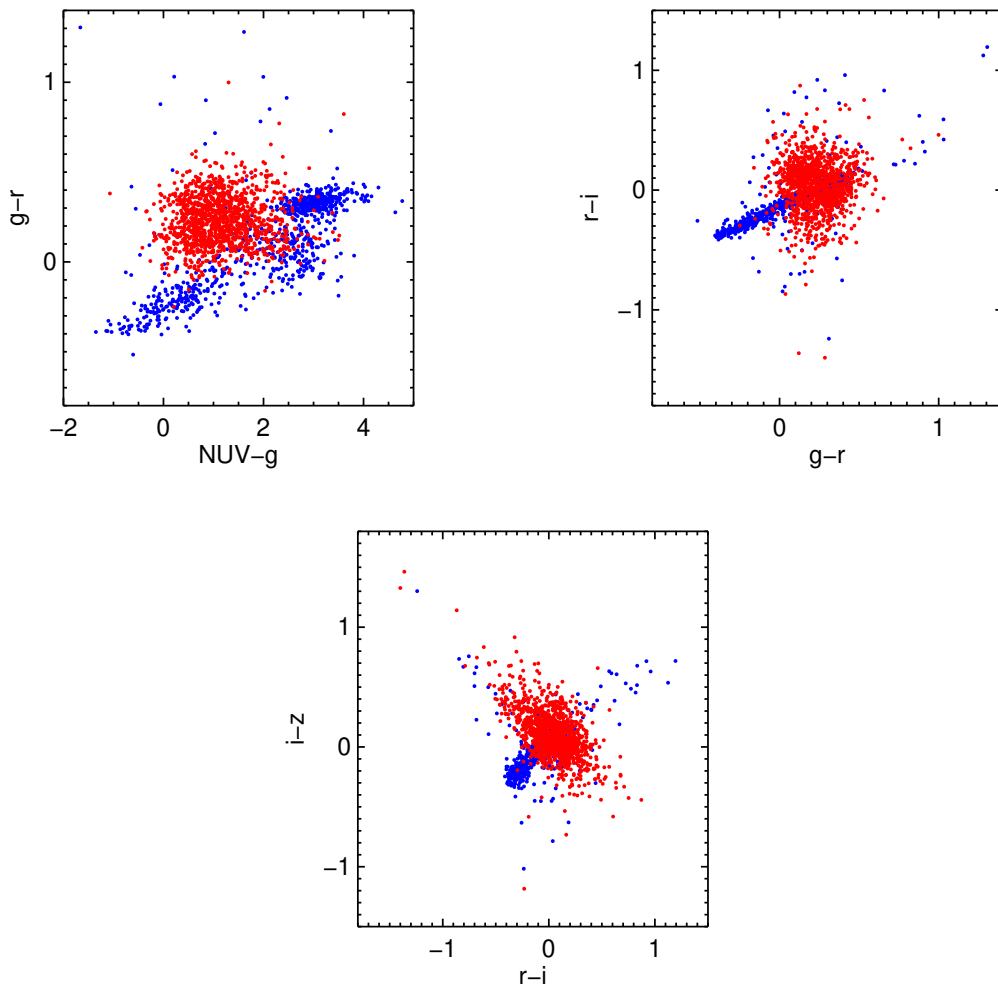


Fig. 5.— Color-color diagrams of the spectroscopically confirmed quasars (red) and stars (blue) in RCS-2. The upper diagrams show the new color NUV-g vs  $g-r$  (left), and  $g-r$  vs  $r-i$  (right), whilst the bottom diagram shows the colors  $r-i$  vs  $i-z$ . As we can see, with the addition of the NUV band there is a clearer separation between quasars and stars in that diagram.

### 3.1.3. Training Set 3 (TrS3)

This training set is also a subset from TrS1, and is built by cross-identifying all quasars and stars from TrS1 with WISE sources detected in the W1 ( $3.4 \mu m$ ) and W2 ( $4.6 \mu m$ ) bands. The  $2''.0$  cross-matching search radius was chosen according to the angular resolution of both catalogs. We use these bands following Stern et al. (2012), where they are used to select quasars from WISE. We additionally make a cut in the magnitude error corresponding to 0.2 in both bands, consistent

with the magnitude limits of our sample. Following these selection criteria, we obtain a sample of 2,748 quasars and 2,679 stars. As can be seen in Figure 8, use of the WISE bands is useful because separation between quasars and stars in the color-color plots is cleaner than those using purely optical RCS-2 bands. We expect, therefore, that inclusion of these bands would boost the performance of the classifier.

One additional advantage in using WISE bands, in common with TrS2, is the introduction of new

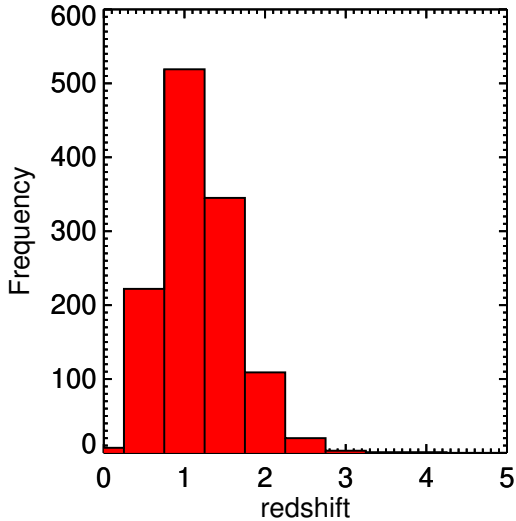


Fig. 6.— Histogram of the redshift distribution of quasars from TrS2.

bands (two in this case) resulting in higher quality classification. Advantages of TrS3 over TrS2 is the additional band available to the algorithm but also the wider redshift coverage, as seen in Figure 9: redshift coverage is complete up to  $z \sim 2$ , yet there are still detections up to  $z \sim 4$ . As such, we are able to classify objects to higher redshifts than in TrS2. Most significantly, WISE detections cover the aforementioned mid-redshift range ( $2.2 \lesssim z \lesssim 3.5$ ), where it is hard to separate quasars from stars. For putative QSOs in this redshift range, the algorithm used in conjunction with TrS3 will be of great use.

Features of the training set utilised by the algorithm are magnitudes in the four RCS2 bands: g, r, i, and z; W1 and W2 magnitudes from WISE; and the colors g-r, g-i, g-z, g-W1, g-W2, r-i, r-z, r-W1, r-W2, i-z, i-W1, i-W2, z-W1, z-W2, and W1-W2. As explained for the previous training sets, we make available all colors to the algorithm.

### 3.2. Data Set

A data set is a sample of point sources for which the class is not known, and where the trained classification model is applied. We have three data sets, one data set for each one of the training sets described above. They are all constructed with

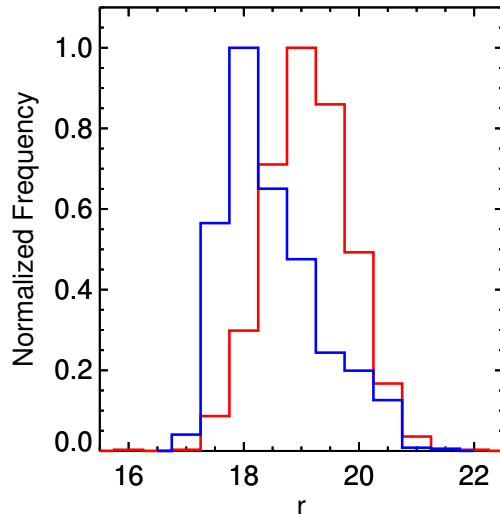


Fig. 7.— Histogram of the normalized magnitude distribution in the r band from RCS-2 of quasars and stars from TrS2. Quasars are in red and stars are in blue.

point sources from RCS-2 photometry with the same requirements as in the training sets.

#### 3.2.1. Data Set 1 (DS1)

This data set is classified using the algorithm trained by TrS1. It includes point sources from RCS-2 that meet the requirements described above. These conditions are imposed for consistency with the TrS1. There are 1,863,970 point sources that the algorithm must classify in this set.

#### 3.2.2. Data Set 2 (DS2)

This data set is classified using the algorithm trained by TrS2. It contains point sources from the previous test set that additionally have *GALEX* NUV-band detections. The matching radius and photometric error limits are the same than TrS2 as described in Section §3.1.2. Within this dataset, there are 16,898 sources the algorithm must classify.

#### 3.2.3. Data Set 3 (DS3)

This data set is classified using the algorithm trained by TrS3. The point sources are those from

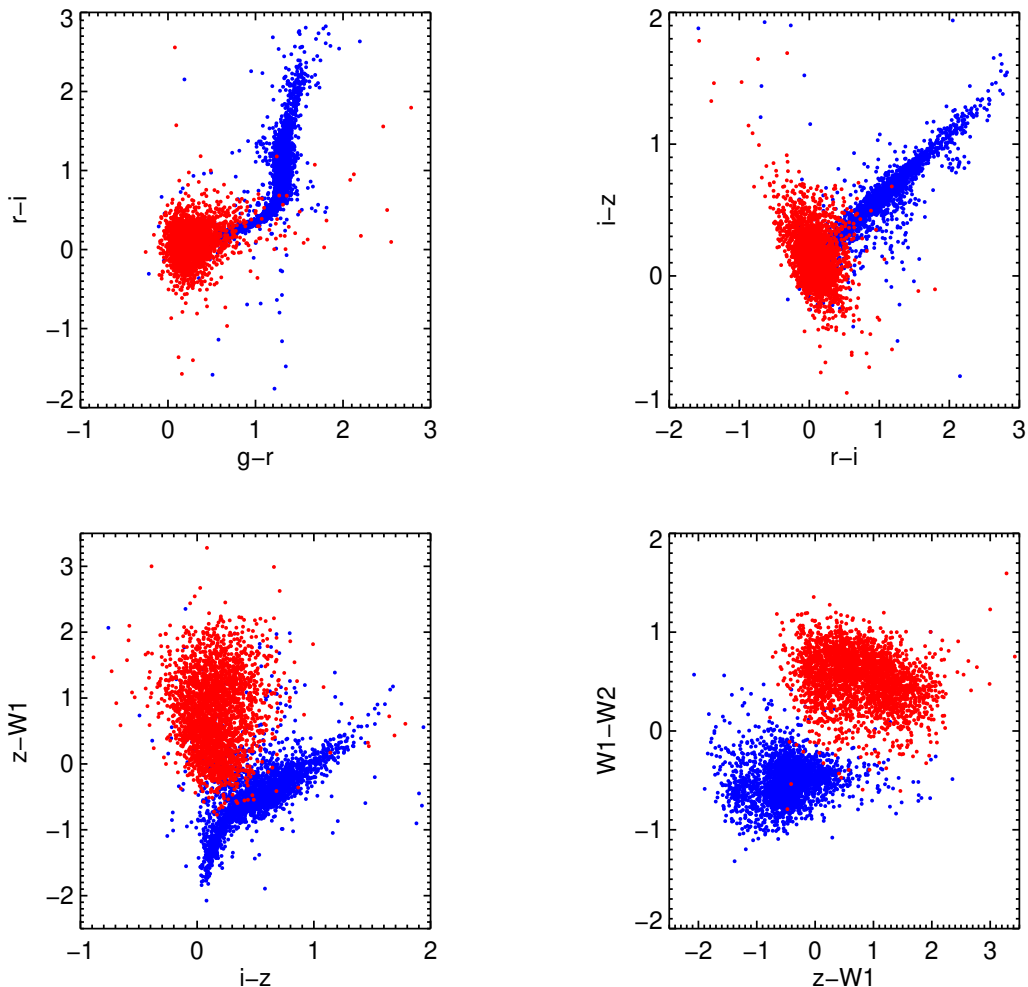


Fig. 8.— Color-color diagrams of the spectroscopically confirmed quasars (red) and stars (blue) in RCS-2 with detection in the W1 and W2 bands from WISE. The upper left diagram shows the colors  $g-r$  vs  $r-i$ , the upper right diagram shows the colors  $r-i$  vs  $i-z$ , the bottom left diagram shows the colors  $i-z$  vs  $z-W1$ , and the bottom right diagram shows the color  $z-W1$  vs  $W1-W2$ . The inclusion of the two new bands makes the overlap between quasars and stars almost disappear.

TeS1 with detection in the W1 and W2 bands from WISE. We apply the TrS3 criteria to the point source catalog for the cross/match and the limit in photometric errors. These constraints result in a data set of 242,902 point sources to classify. The magnitude distribution of this sample is shown in Figure 10. This set is, in average, brighter than TrS1 (around 1 magnitude) but fainter than TrS2 (around 0.5 magnitudes).

#### 4. Results

We train the algorithm with the three training sets separately and then apply it to the corresponding data sets:

- For TrS1, the optimal pair of parameters is  $F = 3$  and  $T = 70$ . The *recall* and *precision* for both classes are shown in Table 2, and the *F-score* is 88.8%. We subsequently

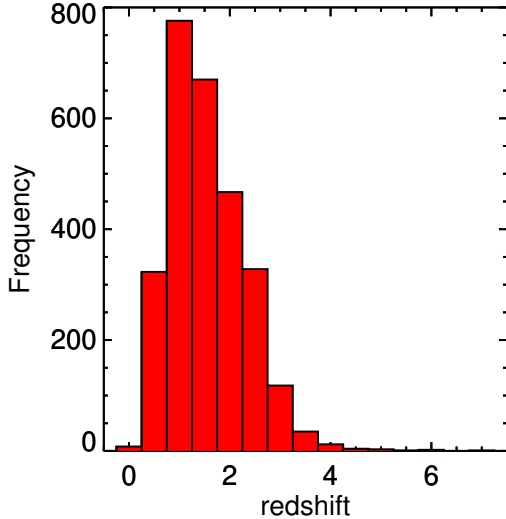


Fig. 9.— Histogram of the redshift distribution of the quasars TrS3.

apply this model to DS1 and obtain 85,085 quasars, which is 4.6% of the total amount of objects.

Figure 11 shows the r-band magnitude distribution of the classified objects. As we see, the number of quasars decays for faint magnitudes ( $r \gtrsim 22$ ) just as expected from the training set. We also see stellar sources much fainter than in the training set (up to  $r \sim 23$ ), consistent with the inclusion of artificial stars. We know this spurious result arises purely from the addition of such stars, and serves to minimize the misidentification of stellar sources as QSOs.

We can compare these results to expectations from the LSST (LSST Science Collaboration et al. 2009), where  $\sim 150,000$  quasars are predicted for our limiting magnitude of  $r = 23$  for the area we are covering. Whilst this is a larger yield than from RCS-2 using our approach, it is consistent when considering our prioritization of *precision* (catalogue purity) rather than *recall* (completeness).

- For TrS2, we find that the optimal param-

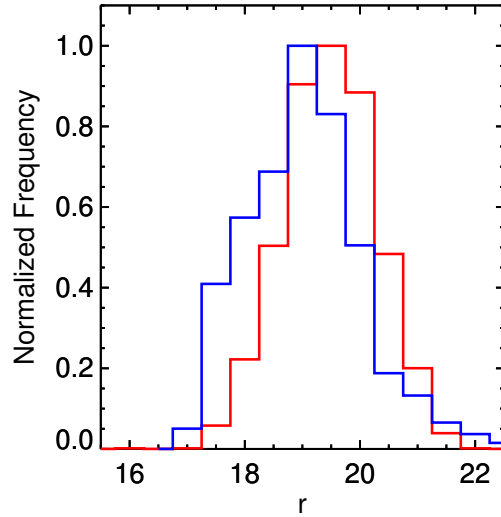


Fig. 10.— Histogram of the normalized magnitude distribution in the r band from RCS-2 of quasars and stars from TrS3. Quasars are in red and stars are in blue.

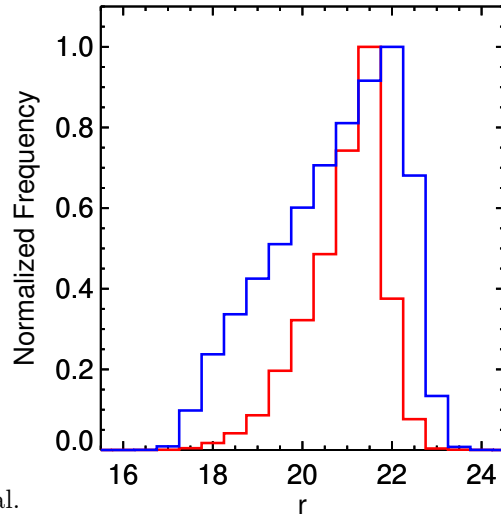


Fig. 11.— Histogram of the normalized r-band magnitude distribution from quasar and star candidates from DS1. Quasars are in red and stars are in blue.

eters for source classification are  $F = 9$  and  $T = 100$ . The *recall* and *precision* resulting

from these parameters are shown in Table 2, and the  $F$ -score is 97.2%. Classifying the objects from DS2 we obtain 6,556 quasars, corresponding to 38.8% of the objects.

As with DS1, in Figure 12 we show the r-band magnitude distribution for objects classified as stars and QSOs; it can be seen that the whole sample is brighter than the first one, as expected. Moreover there is a noted similarity between this distribution and that of the TrS2 in Figure 7.

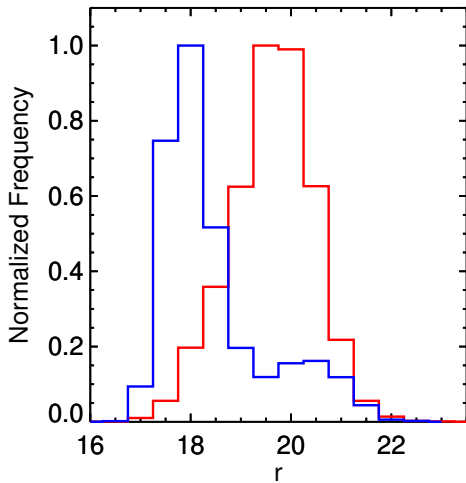


Fig. 12.— Histogram of the normalized magnitude distribution in the r band from quasar and star candidates from DS2. Quasars are in red and stars are in blue.

- For TrS3, we find the best parameters to be  $F = 7$  and  $T = 60$ . The results of *recall* and *precision* are shown in Table 2, and the  $F$ -score is 99.2%. From the DS3 point sources 21,713 are classified as quasars, corresponding to a 8.9% of the total.

Figure 13 shows the r-band magnitude distribution of the classified objects, and as in the training sets, this sample reaches fainter magnitudes than DS2, but is brighter than the DS1. Again, the quasars yield cannot be compared to the LSST prediction.

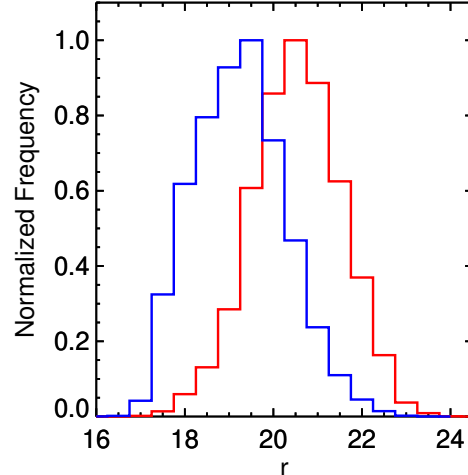


Fig. 13.— Histogram of the normalized magnitude distribution in the r band from quasar and star candidates from DS3. Quasars are in red and stars are in blue.

The total sample of point sources classified was 1,863,970. Of these 16,898 have detection in the NUV band from *GALEX*, and 242,902 have W1 and W2-band WISE detections within the stipulated magnitude error limits. We find that there are 3,600 objects classified as quasars from all three test sets. This low number is anticipated because so few objects from the total sample are detected in the NUV band (the second training set is the smallest one), and even fewer sources have detections in both WISE and *GALEX*. For the same reason, these objects are more likely to be quasars, because they are classified as quasars from three different training sets. Some objects were classified as quasars from two of the three data sets. They correspond to 13,691 distinct sources (11,574 are in DS1 and DS2, 748 in DS1 and DS3, and 1,369 are in DS2 and DS3). The remaining category of quasar classifications were those arising from just one of the three data sets: these comprised a total of 74,551, with 68,542 solely from DS1, 839 from DS2, and 5,170 from DS3. Combining these classifications, we arrive at 91,842 new quasar candidates from RCS-2. The majority of these quasars arise via classifications purely from

DS1; they lack detections in the other bands, and as such are assigned a low priority. We note also a significant number of objects classified as QSOs in DS3 but not DS1. This may be arise from the more conservative classification in DS1 designed to avoid stars that are more numerous in that dataset. However, the inclusion of WISE bands for quasar classification serves the algorithm well, and allows us to increase our overall *recall*.

For each quasar candidate, we construct a catalog containing the coordinates from RCS-2 survey, magnitudes in all the bands in which they have detected in (g, r, i, z, NUV, W1, and W2), photometric errors for those bands, chip number in RCS-2 and a priority. The priority is a measurement of how reliable the quasar classification is, going from 1 (the most reliable) to 3 (the least reliable). The sources assigned priority 1 are those classified as quasars in all three of the test sets. Priority 2 indicates objects classified as quasars in two test sets. Finally, priority 3 is assigned to objects classified from just one test set. Low priorities do not necessarily mean that sources are less likely to be quasars. Some objects may not have detection in WISE or *GALEX* due to low resolution of the surveys, or for example the redshift of the objects. Nevertheless, this indicator is useful in the case of high priority quasars. For example, for spectroscopic confirmation of a limited number of the targets, the priority 1 objects are very likely to be quasars since they have been selected from different training sets.

In tables 1 and 2 we summarize the process:

	TrS1	TrS2	TrS3
N Quasars TrS	4,916	1,228	2,748
N Stars TrS	14,595	815	2,679

Table 1: Summary of the training sets (TrS1, TrS2 and TrS3) used in the Random Forest algorithm.  $N$  Quasars TrS and  $N$  Stars TrS are the number of quasars and stars in the respective training set.

## 5. Spectroscopic confirmation

An important step in validating the catalog constructed in section 4 is through spectroscopic confirmation of our candidates. To painstakingly take spectra for all putative QSOs would be too

	DS1	DS2	DS3
N DS	1,863,970	16,898	242,902
Precision Q (%)	90.4	96.9	99.3
Recall Q (%)	87.3	97.6	99.2
Precision S (%)	95.8	96.3	99.2
Recall S (%)	96.9	95.3	99.3
N Quasars	85,085	6,556	21,713
% Quasars	4.6	38.8	8.9

Table 2: Summary of the Random Forest algorithm applied to RCS-2 point sources for the three data sets.  $N$  DS is the number of objects from the data set. *Precision Q*, *Recall Q*, *Precision S*, and *Recall Q* are the *precision* for quasars, *recall* for quasars, *precision* for stars, and *recall* for stars, respectively.  $N$  Quasars is the number of objects classified as quasars from the data set, and % Quasars is the percentage of those classified quasars from all the objects of the data set.

time-consuming. Instead, we randomly sample sources from the catalog with  $r \leq 19$  that were classified as quasars in at least 2 of the test sets. This bright magnitude limit was chosen such that with a modest telescope, observation of many targets was feasible.

Our observations were carried out at the DuPont telescope (2.5 meters) at Las Campanas Observatory. The Boller & Chivens Spectrograph was used to take long-slit spectra of the targets. The wavelength range, 6230 Å, was adopted in order to cover the largest redshift interval. From our priority 1 and 2 subsamples we measured the spectra of 17 targets. Whilst only a small sample and obviously insufficient for detailed statistical analysis, it nevertheless provides an initial proof-of-concept of the Random Forest algorithm applied to quasar classification. Results of the observations are summarized in Table 3. The reduced spectra of the confirmed quasars are shown in Figure 14

We note that 13 of the 17 candidates are confirmed quasars. Of the remaining objects, one cannot be classified as spectral features could not be identified.

Despite our small sample size preventing detailed statistical insight, we nevertheless consider our

Object	r mag	C1	C2	C3	Priority	Spec	Redshift
RCS2 1243-0438	17.45	Q	Q	Q	1	Quasar	0.78
RCS2 1301-0507	17.90	Q	Q	Q	1	Quasar	0.90
RCS2 1307-0439	18.01	Q	-	Q	2	Quasar	1.2
RCS2 1312-0447	17.75	Q	Q	Q	1	Quasar	0.52
RCS2 1250-0443	18.15	Q	Q	Q	1	Quasar	1.80
RCS2 1251-0435	18.20	Q	Q	Q	1	Quasar	1.63
RCS2 1252-0524	18.00	Q	-	Q	2	Quasar	2.25
RCS2 1301-0518	18.51	Q	Q	Q	1	Galaxy	0.14
RCS2 1303-0448	18.53	Q	-	Q	2	Quasar	2.36
RCS2 1304-0456	18.34	Q	Q	Q	1	Quasar	0.76
RCS2 1057-0448	17.62	Q	Q	Q	1	Quasar	0.68
RCS2 1100-0313	18.18	Q	Q	Q	1	Star	-
RCS2 1101-0846	18.18	Q	Q	Q	1	Quasar	0.38
RCS2 1106-0821	18.19	Q	Q	Q	1	Quasar	1.4/0.6
RCS2 1310-0458	18.40	Q	-	Q	2	Quasar	2.60
RCS2 1308-0505	18.64	Q	-	Q	2	-	-
RCS2 1305-0435	18.48	Q	Q	Q	1	Galaxy	-

Table 3: Spectroscopically confirmed quasar candidates. *Object* is the RCS-2 name. *r mag* is the RCS-2 r band magnitude. *C1*, *C2*, *C3* are the classification in TeS1, TeS2, and TeS3, respectively. Q denotes that it is classified as a quasar in the data set, and ‘-’ means that it is not detected in the respective survey. *Spec* is the spectroscopic classification of the object, and *Redshift* is the spectroscopic redshift.

results satisfactory. It is important to note that in the bright regime we spectroscopically followed, there are more sources in the training sets. Therefore, under the conditions of a complete training set, the algorithm performs very well. We particularly draw attention to the identification of 3 QSOs between  $2.2 \lesssim z \lesssim 3.5$ . It is in this regime that stellar and quasar populations overlap in color-color space.

## 6. Summary and Discussion

Based on a Random Forest algorithm, we built a catalog containing 91,842 new quasar candidates, with a *precision* over 90%. A subset of these, 15% of the quasar catalog, have photometric detections in *GALEX* and/or WISE) and accordingly achieve *precisions* of at least  $\sim 97\%$ . The increase in *precision* with additional bands is anticipated, as the Random Forest algorithm performance improves when more information is provided. This is only significant, however, when that information assists in the separation of the object classes: the additional bands in this 15%

subset assist in separating quasars from stars in color-color space, as seen in Figures 7 and 10). The algorithm, trained with a catalog of spectroscopically-confirmed stars and quasars, is applied to RCS-2 point sources. We require that these point sources have fluxes in all four RCS-2 bands, with photometric errors below 0.1 magnitudes. From these point sources, three data sets (DS1-3) are compiled. The first (DS1) contains all point sources from RCS-2 with the aforementioned requirements. The second (DS2), a subset of DS1, contains RCS-2 point sources with NUV-band *GALEX* detections. The third (DS3), also a subset of DS1, contains RCS-2 point sources with detections in the W1 and W2 WISE bands. We construct quasar catalogs for each of these data sets. The first, with 85,085 quasar classifications from a total of 1,863,970 point sources, corresponds to 4.55 % of the sample. DS2 has 6,556 quasar candidates from 16,898 point sources (38.8% of the total sample). DS3 features 21,713 quasar candidates from 242,902 point sources, corresponding to 8.94% of the data set. Merging quasar classifications from these data sets and removing duplicates, we arrive at a final sample of

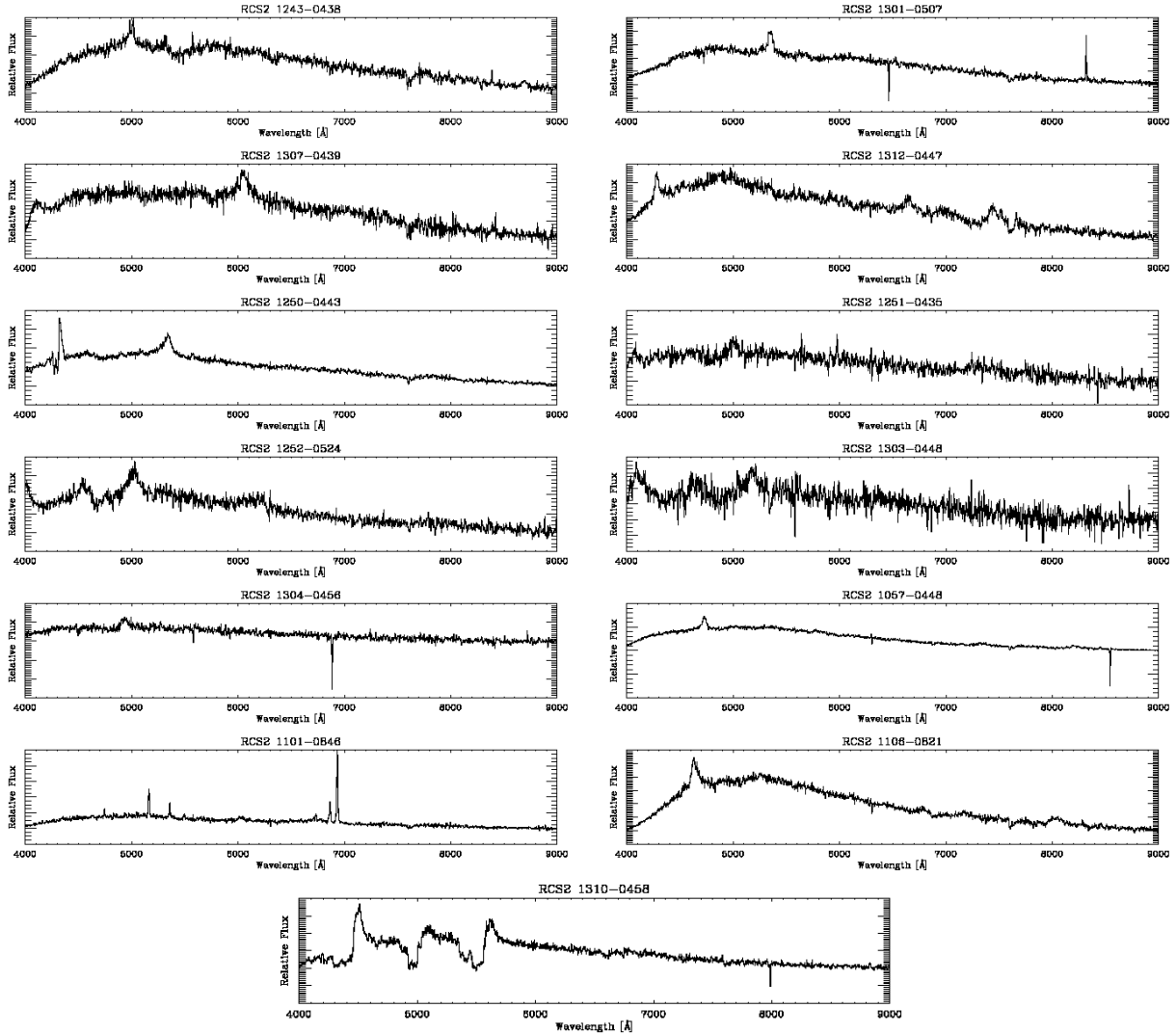


Fig. 14.— Reduced spectra of the confirmed quasars from Table 3.

91,842 quasar candidates. The catalog contains the coordinates from RCS-2 survey, magnitude in all detected bands (NUV, g, r, i, z, W1, W2), photometric errors of those magnitudes, and priority. The priority indicates the reliability of the object classification. Running from 1 to 3, Priority 1 objects have been classified quasars in each of the three data sets, suggesting a secure classification. Priority 2 classifications are those with quasar classification in two of the three data sets, whilst the lowest priority have a classification from just one of the data sets. This latter case does not however suggest the classification is questionable,

merely that they (for example) have no WISE or *GALEX* data. Nevertheless, the Priority is a useful indicator when seeking candidates that have the highest probability of being genuine quasars. We have obtained a reliable new sample of quasars that can be used for a wide range of applications. From this sample, we obtained spectra of 17 candidates with magnitudes  $r \sim 19$ , and priority 1 or 2. From this small sample, 13 are confirmed to be quasars. Even within this small sample, there is good agreement with our expectations. Random Forest works well in the classification of point sources into quasars and stars based on

magnitude and color information. The algorithm is useful because it autonomously chooses the attributes that separate the classes in an optimal way. The approach has broad applicability, permitting a similar studies on future surveys such as LSST, requiring only a training set and photometric information. The advantage of the Random Forest over many other approaches is its high level of automatization and suitability in processing large volumes of data. Training sets need be neither new or large - spectroscopically confirmed SDSS sources were entirely suitable for our purposes in this study. Extensions to the work detailed here could simply be application of the existing algorithm and training sets to new, larger photometric catalogs needing classification.

## 7. Acknowledgments

This paper is supported by the Chilean Ministry for the Economy, Development, and Tourism's Programa Iniciativa Científica Milenio through grant P07-021-F, awarded to The Milky Way Millennium Nucleus. We also acknowledge financial support from Proyecto Financiamiento Basal PFB06, Gemini Conicyt grant 32110010, Programa de Postgrado Instituto de Astrofísica and from BASAL PFB-06, and FONDEF D11I1060. L. F. Barriento's research is supported by proyecto FONDECYT 1120676 and by the Ministry for the Economy, Development, and Tourism's Programa Iniciativa Científica Milenio through grant IC 12009, awarded to The Millennium Institute of Astrophysics (MAS).

## REFERENCES

- C. P. Ahn, R. Alexandroff, C. Allende Prieto, et al. The Ninth Data Release of the Sloan Digital Sky Survey: First Spectroscopic Data from the SDSS-III Baryon Oscillation Spectroscopic Survey. *ApJS*, 203:21, Dec. 2012. doi: 10.1088/0067-0049/203/2/21.
- N. M. Ball & R. J. Brunner. Data Mining and Machine Learning in Astronomy. *International Journal of Modern Physics D*, 19:1049–1106, 2010. doi: 10.1142/S0218271810017160.
- N. M. Ball, R. J. Brunner, A. D. Myers, & D. Tchong. Robust Machine Learning Applied to Astronomical Data Sets. I. Star-Galaxy Classification of the Sloan Digital Sky Survey DR3 Using Decision Trees. *ApJ*, 650:497–509, Oct. 2006. doi: 10.1086/507440.
- N. M. Ball, R. J. Brunner, A. D. Myers, et al. Robust Machine Learning Applied to Astronomical Data Sets. II. Quantifying Photometric Redshifts for Quasars Using Instance-based Learning. *ApJ*, 663:774–780, July 2007. doi: 10.1086/518362.
- R. H. Becker, R. L. White, M. D. Gregg, et al. The FIRST Bright Quasar Survey. III. The South Galactic Cap. *ApJS*, 135:227–262, Aug. 2001. doi: 10.1086/321798.
- J. Bovy, J. F. Hennawi, D. W. Hogg, et al. Think Outside the Color Box: Probabilistic Target Selection and the SDSS-XDQSO Quasar Targeting Catalog. *ApJ*, 729:141, Mar. 2011. doi: 10.1088/0004-637X/729/2/141.
- L. Breiman. Random forests. In *Machine Learning*, pages 5–32, 2001.
- J. A. Cardelli, G. C. Clayton, & J. S. Mathis. The relationship between infrared, optical, and ultraviolet extinction. *ApJ*, 345:245–256, Oct. 1989. doi: 10.1086/167900.
- A. Collister, O. Lahav, C. Blake, et al. MegaZLRG: a photometric redshift catalogue of one million SDSS luminous red galaxies. *MNRAS*, 375:68–76, Feb. 2007. doi: 10.1111/j.1365-2966.2006.11305.x.
- C. Cortes & V. Vapnik. Support-vector networks. In *Machine Learning*, pages 273–297, 1995.
- P. Dubath, L. Rimoldini, M. Süveges, et al. Random forest automated supervised classification of Hipparcos periodic variable stars. *MNRAS*, 414:2602–2617, July 2011. doi: 10.1111/j.1365-2966.2011.18575.x.
- R. O. Duda & P. E. Hart. *Pattern classification and scene analysis*. 1973.
- S. Eales, L. Dunne, D. Clements, et al. The Herschel ATLAS. *PASP*, 122:499–515, May 2010. doi: 10.1086/653086.

- X. Fan. Simulation of Stellar Objects in SDSS Color Space. *AJ*, 117:2528–2551, May 1999. doi: 10.1086/300848.
- C. Faure, T. Anguita, A. Eigenbrod, et al. Redshifts and lens profile for the double quasar QJ 0158-4325. *A&A*, 496:361–364, Mar. 2009. doi: 10.1051/0004-6361:200810277.
- C. B. Foltz, F. H. Chaffee, P. C. Hewett, et al. The large, bright QSO survey. II - QSOs in three equatorial fields. *AJ*, 98:1959–1988, Dec. 1989. doi: 10.1086/115271.
- M. Fukugita, T. Ichikawa, J. E. Gunn, et al. The Sloan Digital Sky Survey Photometric System. *AJ*, 111:1748, Apr. 1996. doi: 10.1086/117915.
- D. W. Gerdes, A. J. Sypniewski, T. A. McKay, et al. ArborZ: Photometric Redshifts Using Boosted Decision Trees. *ApJ*, 715:823–832, June 2010. doi: 10.1088/0004-637X/715/2/823.
- D. G. Gilbank, M. D. Gladders, H. K. C. Yee, & B. C. Hsieh. The Red-sequence Cluster Survey-2 (RCS-2): Survey Details and Photometric Catalog Construction. *AJ*, 141:94, Mar. 2011. doi: 10.1088/0004-6256/141/3/94.
- E. Glikman, D. J. Helfand, R. L. White, et al. The FIRST-2MASS Red Quasar Survey. *ApJ*, 667:673–703, Oct. 2007. doi: 10.1086/521073.
- R. F. Green, M. Schmidt, & J. Liebert. The Palomar-Green catalog of ultraviolet-excess stellar objects. *ApJS*, 61:305–352, June 1986. doi: 10.1086/191115.
- M. D. Gregg, R. H. Becker, R. L. White, et al. The First Bright QSO Survey. *AJ*, 112:407, Aug. 1996. doi: 10.1086/118024.
- P. C. Hewett, C. B. Foltz, & F. H. Chaffee. The large bright quasar survey. 6: Quasar catalog and survey parameters. *AJ*, 109:1498–1521, Apr. 1995. doi: 10.1086/117380.
- P. F. Hopkins, L. Hernquist, T. J. Cox, B. Robertson, & V. Springel. Determining the Properties and Evolution of Red Galaxies from the Quasar Luminosity Function. *ApJS*, 163:50–79, Mar. 2006. doi: 10.1086/499493.
- M. Huertas-Company, D. Rouan, L. Tasca, G. Soucail, & O. Le Fèvre. A robust morphological classification of high-redshift galaxies using support vector machines on seeing limited images. I. Method description. *A&A*, 478:971–980, Feb. 2008. doi: 10.1051/0004-6361:20078625.
- T. H. Jarrett, M. Cohen, F. Masci, et al. The Spitzer-WISE Survey of the Ecliptic Poles. *ApJ*, 735:112, July 2011. doi: 10.1088/0004-637X/735/2/112.
- N. Kaiser, H. Aussel, B. E. Burke, et al. Pan-STARRS: A Large Synoptic Survey Telescope Array. In J. A. Tyson & S. Wolff, editors, *Survey and Other Telescope Technologies and Discoveries*, volume 4836 of *Society of Photo-Optical Instrumentation Engineers (SPIE) Conference Series*, pages 154–164, Dec. 2002. doi: 10.1117/12.457365.
- S. Lopez, L. F. Barrientos, P. Lira, et al. Galaxy Clusters in the Line of Sight to Background Quasars. I. Survey Design and Incidence of Mg II Absorbers at Cluster Redshifts. *ApJ*, 679:1144–1161, June 2008. doi: 10.1086/587678.
- LSST Science Collaboration, P. A. Abell, J. Allison, et al. LSST Science Book, Version 2.0. *ArXiv e-prints*, Dec. 2009.
- D. C. Martin, J. Fanson, D. Schiminovich, et al. The Galaxy Evolution Explorer: A Space Ultraviolet Survey Mission. *ApJ*, 619:L1–L6, Jan. 2005. doi: 10.1086/426387.
- M. Oguri, N. Inada, M. A. Strauss, et al. The Sloan Digital Sky Survey Quasar Lens Search. III. Constraints on Dark Energy from the Third Data Release Quasar Lens Catalog. *AJ*, 135:512–519, Feb. 2008. doi: 10.1088/0004-6256/135/2/512.
- K. Pichara & P. Protopapas. Automatic Classification of Variable Stars in Catalogs with Missing Data. *ApJ*, 777:83, Nov. 2013. doi: 10.1088/0004-637X/777/2/83.
- K. Pichara, P. Protopapas, D.-W. Kim, J.-B. Marquette, & P. Tisserand. An improved quasar detection method in EROS-2 and MACHO LMC data sets. *MNRAS*, 427:1284–1297, Dec. 2012. doi: 10.1111/j.1365-2966.2012.22061.x.

- L. Portinari, J. Kotilainen, R. Falomo, & R. Decarli. On the cosmological evolution of the black hole-host galaxy relation in quasars. *MNRAS*, 420:732–744, Feb. 2012. doi: 10.1111/j.1365-2966.2011.20086.x.
- J. R. Quinlan. *C 4.5: Programs for machine learning*. 1993.
- G. T. Richards, X. Fan, D. P. Schneider, et al. Colors of 2625 Quasars at  $0 < Z < 5$  Measured in the Sloan Digital Sky Survey Photometric System. *AJ*, 121:2308–2330, May 2001. doi: 10.1086/320392.
- G. T. Richards, X. Fan, H. J. Newberg, et al. Spectroscopic Target Selection in the Sloan Digital Sky Survey: The Quasar Sample. *AJ*, 123:2945–2975, June 2002. doi: 10.1086/340187.
- J. W. Richards, D. L. Starr, N. R. Butler, et al. On Machine-learned Classification of Variable Stars with Sparse and Noisy Time-series Data. *ApJ*, 733:10, May 2011. doi: 10.1088/0004-637X/733/1/10.
- D. E. Rumelhart, G. E. Hinton, & R. J. Williams. Learning representations by back-propagating errors. *Nature*, 323:533–536, Oct. 1986. doi: 10.1038/323533a0.
- D. B. Sanders, E. S. Phinney, G. Neugebauer, B. T. Soifer, & K. Matthews. Continuum energy distribution of quasars - Shapes and origins. *ApJ*, 347:29–51, Dec. 1989. doi: 10.1086/168094.
- D. J. Schlegel, D. P. Finkbeiner, & M. Davis. Maps of Dust Infrared Emission for Use in Estimation of Reddening and Cosmic Microwave Background Radiation Foregrounds. *ApJ*, 500:525, June 1998. doi: 10.1086/305772.
- D. Stern, R. J. Assef, D. J. Benford, et al. Mid-infrared Selection of Active Galactic Nuclei with the Wide-Field Infrared Survey Explorer. I. Characterizing WISE-selected Active Galactic Nuclei in COSMOS. *ApJ*, 753:30, July 2012. doi: 10.1088/0004-637X/753/1/30.
- The Dark Energy Survey Collaboration. The Dark Energy Survey. *ArXiv Astrophysics e-prints*, Oct. 2005.
- A. T. Tokunaga & W. D. Vacca. “The Mauna Kea Observatories Near-Infrared Filter Set. III. Isophotal Wavelengths and Absolute Calibration” ([iA href="/abs/2005PASP.117..421T"](/abs/2005PASP.117..421T))<sub>iPASP</sub>, 117, 421 [2005]<sub>i/A<sub>i</sub></sub>). *PASP*, 117:1459–1459, Dec. 2005. doi: 10.1086/499029.
- G. B. Trammell, D. E. Vanden Berk, D. P. Schneider, et al. The UV Properties of SDSS-Selected Quasars. *AJ*, 133:1780–1794, Apr. 2007. doi: 10.1086/511817.
- R. L. White, R. H. Becker, M. D. Gregg, et al. The FIRST Bright Quasar Survey. II. 60 Nights and 1200 Spectra Later. *ApJS*, 126:133–207, Feb. 2000. doi: 10.1086/313300.
- C. J. Willott, X. Delfosse, T. Forveille, P. Delforme, & S. D. J. Gwyn. First Results from the Canada-France High- $z$  Quasar Survey: Constraints on the  $z = 6$  Quasar Luminosity Function and the Quasar Contribution to Reionization. *ApJ*, 633:630–637, Nov. 2005. doi: 10.1086/462408.
- C. Wolf. Bayesian photometric redshifts with empirical training sets. *MNRAS*, 397:520–533, July 2009. doi: 10.1111/j.1365-2966.2009.14953.x.
- E. L. Wright, P. R. M. Eisenhardt, A. K. Mainzer, et al. The Wide-field Infrared Survey Explorer (WISE): Mission Description and Initial On-orbit Performance. *AJ*, 140:1868, Dec. 2010. doi: 10.1088/0004-6256/140/6/1868.
- H. K. C. Yee. A faint-galaxy photometry and image-analysis system. *PASP*, 103:396–411, Apr. 1991. doi: 10.1086/132834.
- H. K. C. Yee, E. Ellingson, & R. G. Carlberg. The CNOC Cluster Redshift Survey Catalogs. I. Observational Strategy and Data Reduction Techniques. *ApJS*, 102:269, Feb. 1996. doi: 10.1086/192259.
- D. G. York, J. Adelman, J. E. Anderson, Jr., et al. The Sloan Digital Sky Survey: Technical Summary. *AJ*, 120:1579–1587, Sept. 2000. doi: 10.1086/301513.

---

This 2-column preprint was prepared with the AAS L<sup>A</sup>T<sub>E</sub>X macros v5.2.